

Seasonal variation of aerosols in the Martian atmosphere

Anthony D. Toigo and Mark I. Richardson

Division of Geological and Planetary Sciences,
California Institute of Technology, Pasadena

Abstract. Reanalysis of Viking Lander (VL) visible and Viking Orbiter infrared optical depth measurements shows that the visible to infrared ratio of total extinction opacity varies with season. The ratio is near to its previously reported constant value, 2.5, during dust storm periods and higher during northern spring and summer. The increase in ratio is hypothesized to be due to seasonally varying water ice haze, which produces a higher optical depth in the visible than in the infrared. This differs significantly from previous analyses of VL visible opacities which have assumed that only dust contributes to the optical depth measured during the early afternoon. Consequently we suggest that the Martian atmosphere is clearer of dust, especially during northern spring and summer, than previously suggested based upon VL data. We find dust visible optical depths of 0.1–0.4 during the northern spring and summer seasons, compared to previous estimates of 0.4–0.6. We also find that water ice hazes can provide roughly 50% of the total visible opacity in these seasons. For southern spring and summer, dust optical depths are more variable, but generally ≥ 0.4 , with water ice opacity ≤ 0.1 . The data suggest water ice optical depths are slightly higher and peak earlier ($L_s=80^\circ\text{--}90^\circ$) at VL1 than at VL2 ($L_s=115^\circ\text{--}130^\circ$). We estimate average northern summer water (daytime minimum) ice masses to be roughly 0.1–0.5 precipitable microns, depending on the assumed particle size distribution and hence 1–5% of the total water column. The observation of significant and previously unrecognized amounts of water ice haze suggests a larger role for water in controlling atmospheric heating rates and the vertical distribution of dust and water vapor than has been widely accepted to date.

1. Introduction

Dust has a profound impact on the Martian atmosphere. It is both an effective absorber of solar radiation and an effective emitter/absorber of thermal infrared radiation. Consequently, the amount and distribution of dust in the atmosphere significantly affects atmospheric heating rates and hence the circulation [Zurek *et al.*, 1992]. Thus characterization of the seasonal dust cycle is of prime importance in understanding the current Martian climate.

The seasonal cycle of dust on Mars is the keystone to the other seasonal cycles because of its impact on atmospheric temperature structure and transport and, through this, its impact on volatile cycles and climate. The current standard view of the dust cycle derives from Viking Lander (VL) measurements of the visible optical depth since the optical depth of the atmosphere provides a measure of the amount of suspended aerosols. The key assumption in the interpretation of these data has been that only dust significantly contributes to the daytime opacity [Pollack *et al.*, 1979; Colburn *et al.*, 1989] and hence that the amount of atmospheric dust can be directly derived from them. However, dust is not the only

aerosol in the Martian atmosphere. Water ice and CO_2 ice particles also form in the atmosphere [Curran *et al.*, 1973; Herr and Pimental, 1969], and while CO_2 ice particle formation is limited to the winter polar regions and high altitudes, water ice particles can form at most latitudes and at most seasons.

The optical depth of the atmosphere has also been measured in the infrared by the Viking Orbiters' Infrared Thermal Mapper (IRTM) instruments [Martin, 1986; Martin and Richardson, 1993]. Through observations of the depth of the $9 \mu\text{m}$ silicate absorption feature relative to the $7 \mu\text{m}$ "continuum" these measurements theoretically allow the derivation of dust optical depth independent of other aerosols. However, water ice particles can affect the infrared opacity, though to a much smaller degree than in the visible. The ratio of dust optical depth in the visible to that in the infrared has physical significance in that the opacity in the visible is a gauge of the effectiveness of solar heating due to dust absorption, while the opacity in the infrared represents the ability of the atmosphere to radiate heat to space through infrared emission by dust. The ratio is also of diagnostic importance as it is sensitive to dust properties. The value of the visible to infrared ratio for dust has typically been taken to be constant at roughly 2.5 [Martin, 1986]. Again assuming that dust is the only aerosol, this fixed value of the opacity ratio has been used in atmospheric circulation model heating rate

calculations as well as to help constrain dust particle properties, such as composition and particle size distribution.

Seasonal variation in this ratio would have a wide range of implications. However, the ratio has not been derived for a good fraction of the annual cycle. Variations in the ratio as a function of season could imply that aerosol populations have been incorrectly assessed in the past (i.e., that neglecting water ice aerosols is not valid), that dust particle size distributions vary significantly, or that our current understanding of the vertical distribution of dust is wrong. In any case, opacity ratio variations reflect variations in atmospheric aerosol properties that are not incorporated in current atmospheric radiative models, and hence, circulation models. We began this study in order to examine any temporal variations in this ratio and found a significant seasonal cycle with northern summer peak values exceeding 20. In section 2 we describe the means by which we derived the ratio and show the seasonal variations. Then, in section 3 we discuss three likely causes for the variation. The options are changes in the dust particle size distribution, changes in the vertical distribution of dust, or variations in the amount of dust and water ice in the atmosphere. Indeed, we conclude that the primary cause must be a significant contribution to opacity by water ice hazes (we use the phrases "water ice," "water ice hazes," and "water ice clouds" interchangeably) during northern spring and summer, arguing that the standard interpretation of VL opacity as being solely a measure of dust must be abandoned. Next, in section 4 we reanalyze the Mars Pathfinder optical depth measurements in terms of the mixed dust/water ice model. In section 5 we discuss our results within the context of a new picture of Mars climate. Finally, in section 6 we review our conclusions, primarily that water ice hazes play a significantly greater role in the seasonal aerosol cycle than has been previously suspected.

2. Data

The most widely reported measurements of the atmospheric optical depth are those derived from the VL cameras. Both landers measured optical depth by directly imaging the Sun at various zenith angles in the broadband solar channel centered on 670 nm [Pollack *et al.*, 1977, 1979; Colburn *et al.*, 1989]. These are shown in Plates 1a and 1d. Data have been filtered to show only the afternoon values where the water ice cloud contribution will be at a minimum [Colburn *et al.*, 1989]. The common assumption is that this minimum corresponds to the absence of water ice clouds and that the opacity observed at these local times is due entirely to dust. The graphs show a relatively clear northern spring and summer ($L_s = 0^\circ - 180^\circ$) with visible optical depths of 0.4–0.7. Values for VL2 are slightly smaller, due to its position at higher elevation and the fact that aerosol opacity roughly scales with atmospheric mass [Kahn *et al.*, 1981]. A more dusty southern spring and summer (northern fall and winter, $L_s = 180^\circ - 360^\circ$) is also apparent, including the two great dust storms of 1977 during which visible optical depths reached values in excess of 3.

The retrieval of optical depth in the infrared (9 μm) from IRTM observations has been described by Martin [1986] and

Martin and Richardson [1993]. Using the corrected IRTM 15 μm brightness (T_{15}) temperatures [Wilson and Richardson, 2000], the surface emissivities of Christensen [1982], and the two-stream source-function radiation code of Zurek [1981], we have rederived the infrared optical depths for the first two Viking years. Additionally, we have modified the two-stream code to treat nonuniform (i.e., non-constant mixing ratio) vertical distributions of dust. Once again, it is common to assume that these infrared opacities are due to atmospheric dust alone. While the effect of water ice on these opacities will certainly be smaller than on the visible opacities, the impact is likely non-negligible and is addressed in section 3. Our derived values of 9 μm optical depths are shown in Plates 1a and 1d in conjunction with the visible opacities. The infrared data shown in Plates 1a and 1d correspond to IRTM observations near both landing sites. The infrared data included in this study fell within a $5^\circ \times 5^\circ$ latitude-longitude box centered on each lander and had emission and incidence angles $< 60^\circ$ (to minimize atmospheric mass effects). The infrared values have been scaled up by the canonical factor of 2.5 to more readily highlight deviations from this assumed constant ratio value. The general cycle of orbiter-derived opacity followed that of the landers.

The ratio of optical depths (visible to infrared) of 2.5 was derived by Martin [1986] by comparing Viking Orbiter and VL data sets during the dusty southern summer period; comparison during the rest of the annual cycle was not pursued due to the "very low opacities in that period" [Martin, 1986, p. 9]. The concern was that random noise in these low-opacity data would make meaningless any comparison with the visible opacities. However, Plates 1a and 1d show that the random variation in opacities is consistently less than the difference between the visible and infrared opacities (even when scaled by 2.5); therefore comparison outside the dust storm season is valid.

A very clear trend in the opacity behavior emerges when the visible and infrared values are compared over the full annual cycle. While the seasonal trends in the visible and infrared optical depths at each landing site are similar, the infrared optical depths are lower during northern spring and summer than the VL values, even after scaling the values by the canonical factor of 2.5.

The error bars for the visible opacity are shown. The error is harder to quantify for the infrared data; however, there is enough infrared data that the random error can be gauged from the scatter of individual data points. Again, it is important to note that the scaled infrared values are consistently lower than the visible values in the northern spring and summer seasons. Even in the unlikely event that the infrared opacities are biased low by the 10–25% error that Martin [1986] quotes, the scaled infrared opacities would still be lower than the visible values.

The derivation of infrared opacities uses the T_{15} temperatures, which have been shown to be biased by surface temperatures during the middle portion of the day [Wilson and Richardson, 2000]. As we derive infrared opacities during the late morning and early afternoon, we have examined the impact of the corrected T_{15} temperatures on the model temperature profile constructed within the optical depth retrieval

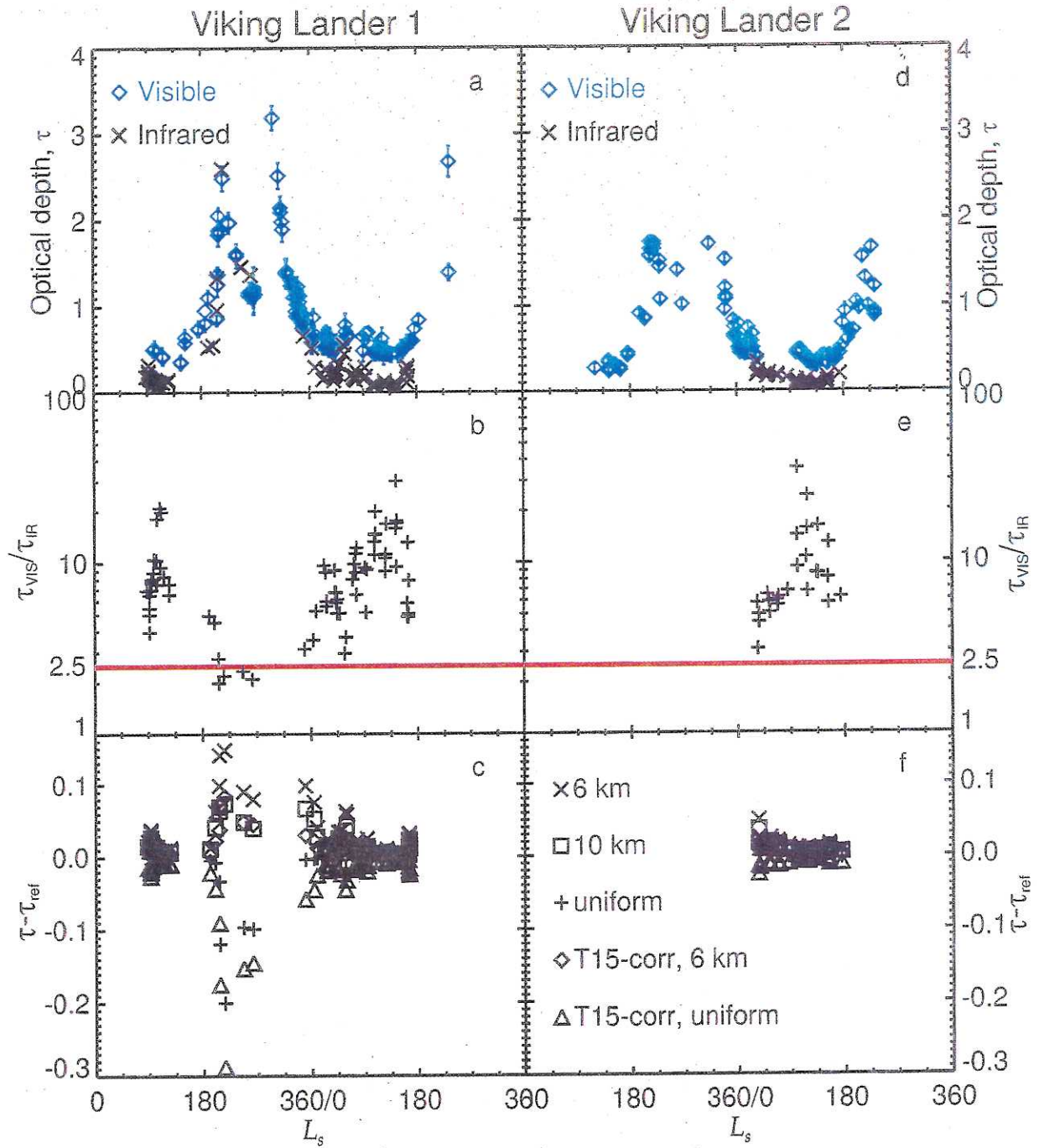


Plate 1. (a) Optical depth versus L_s for the Viking Lander 1 location. L_s values range from 0 to 720, with 360–720 representing the second Martian year of Viking observations. Viking Lander derived values are shown in blue diamonds, with their associated error bars. The Infrared Thermal Mapper (ITRM) derived values are shown as black crosses. The ITRM values have been scaled by a factor of 2.5 to show their good agreement during dusty periods ($L_s=180^\circ$ – 360°) and their lack of agreement during the clear periods ($L_s=0^\circ$ – 180°). (b) Plot of the ratio of visible to infrared optical depths versus L_s for the Viking Lander 1 location. (c) Difference between the derived infrared optical depths for the reference case (using corrected T_{15} temperatures and dust confined to 1 scale height) and optical depths derived for various combinations of corrected and uncorrected T_{15} temperatures and dust distributed uniformly, to 10 km, and to 6 km. (d)–(f) Similar to Plates 1a–1c, respectively, except for the Viking Lander 2 location.

code. The results are shown in Plates 1c and 1f. It can be seen that during relatively dust-free periods the difference between opacities derived using corrected and uncorrected T_{15} temperatures is roughly 10%.

All previous derivations of 9 μm infrared opacity [Martin, 1986; Martin and Richardson, 1993; Fenton et al., 1997] have used a uniform distribution of dust. However, this may not always be appropriate, and so, we have tested the sensi-

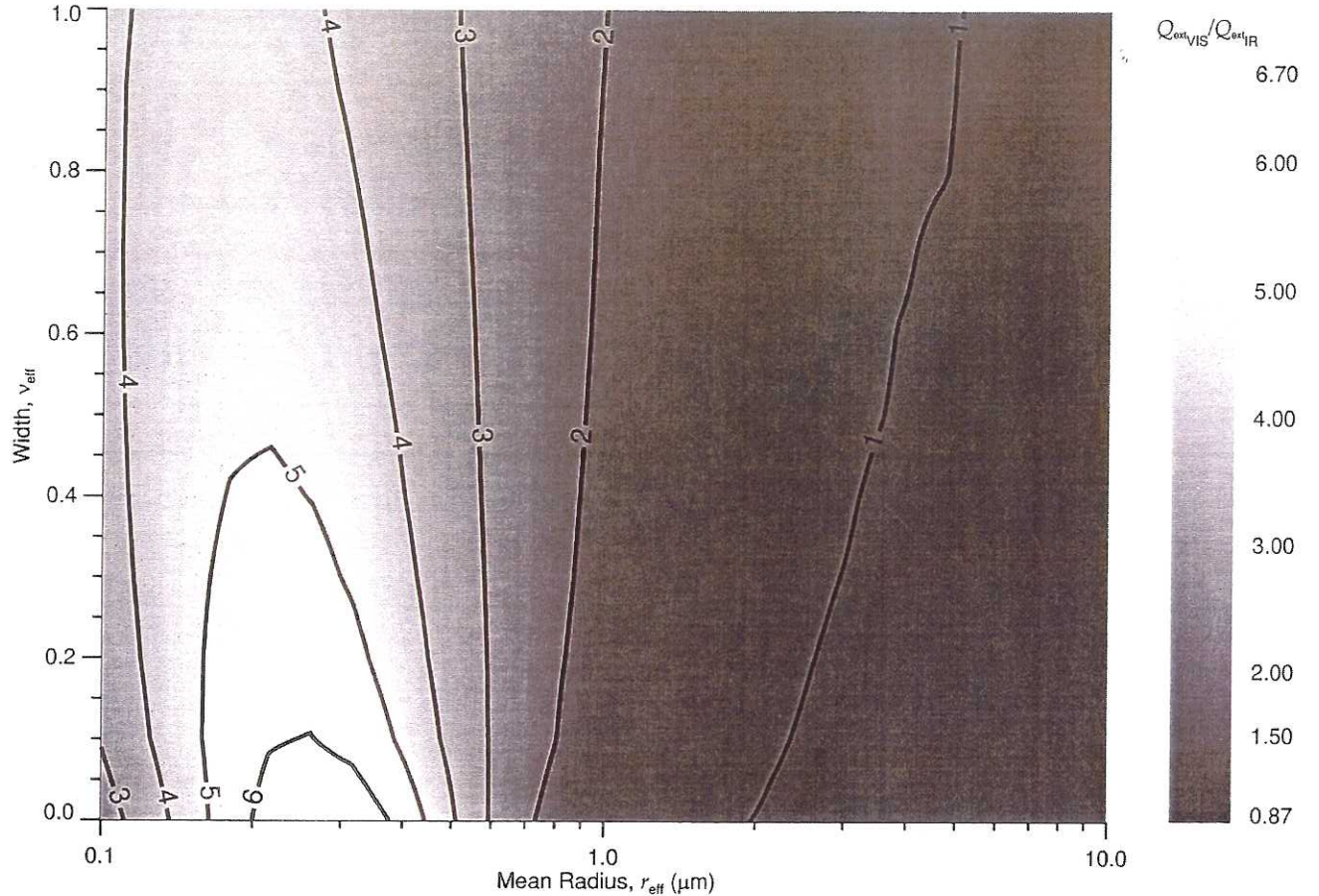


Figure 1. Ratio of optical depths in the visible and infrared as a function of cross-section weighted mean particle size (r_{eff}), in microns, and effective width of the distribution (v_{eff}) for a modified gamma distribution of spherical dust particles. Indices of refraction in the visible came from Ockert-Bell *et al.* [1997] and in the infrared from Toon *et al.* [1977]. Note that modified gamma distribution has three independent variables, α , γ , and r_{mode} (r_{eff} is a function of all three, and v_{eff} is a function of α and γ), one of which is usually held constant. A constant value of $\alpha = 2$ was chosen for consistency with Toon *et al.* [1977] and Pollack *et al.* [1979]. The visible to infrared opacity ratio (as a function of r_{eff} and v_{eff}) is relatively insensitive to the choice of α .

tivity of optical depth retrievals to varying vertical distributions of dust. We chose a vertical distribution of dust that is capped at 10 km as our standard case (the mixing ratio as a function of height was described following Conrath [1975] using $\nu = 0.5$). This height was chosen as it likely represents a realistic lower bound on the depth of dust mixing during the northern spring and summer period [Richardson, 1999]. Additionally, we calculated opacities for a uniform vertical distribution and for an extremely shallow distribution capped at 6 km ($\nu = 1$) (Plates 1c and 1f).

It is clear from Plates 1a and 1d that while a visible to infrared ratio of 2.5 is good for dusty periods (southern spring and summer), the ratio increases significantly during the clearer periods (northern spring and summer). The visible to infrared ratios derived by comparing our infrared observations with those from VL are shown in Plates 1b and 1e. A strong anti-correlation can be seen between the ratio and opacity. The ratio reaches its minimum near 2.5 during the extremely dusty periods and increases both in value and in its variation during the clear periods.

3. Interpretation

There are three possible explanations for the increased ratio during the clear periods: (1) changes in the mean size of suspended dust particles, which would vary the visible to infrared ratio assuming that the total extinction is due to dust, (2) confinement of dust within a shallower layer of the atmosphere, which would produce an underestimate of infrared opacity (and an overestimate of the ratio) when retrieved assuming a uniform vertical distribution of dust, and (3) increased visible opacity due to the presence of previously neglected water ice clouds, while the dust visible to infrared opacity ratio is assumed to remain constant.

3.1. Changes in the Dust Particle Size Distribution

The settling and removal of larger dust particles following dusty periods may result in the shrinking of both the mean size of the particle size distribution and the width of the distribution, leading to increased visible to infrared ratios as the smaller particles exert more influence in the visible wave-

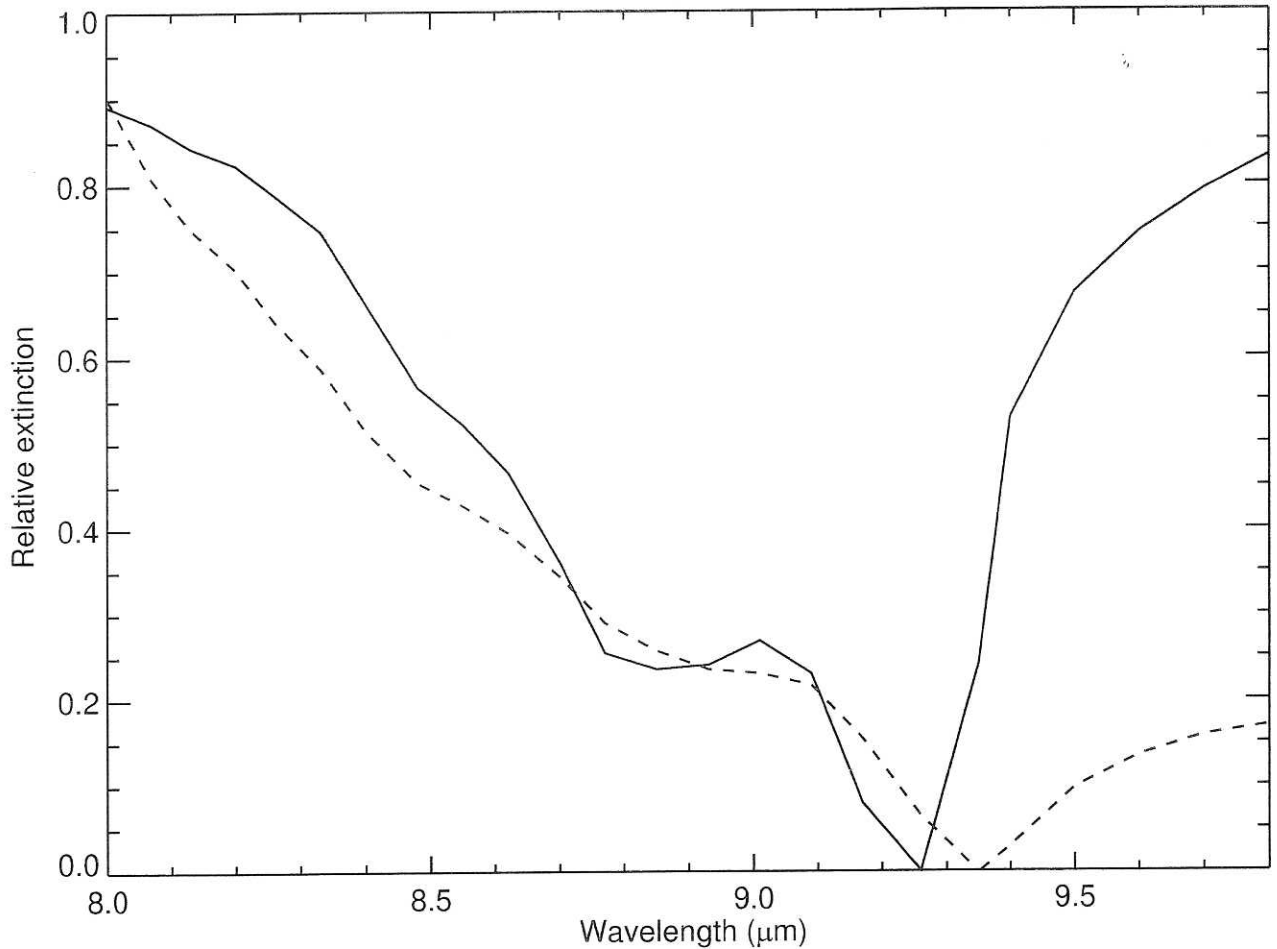


Figure 2. Relative extinction due to dust particles as a function of wavelength, assuming spherical particles. The solid line represents a dust particle size distribution with $r_{\text{eff}} = 0.3 \mu\text{m}$ and $v_{\text{eff}} = 0.0$, which yields a visible to infrared optical depth ratio of approximately 6.5. The dashed line represents a dust particle size distribution with $r_{\text{eff}} = 1.8 \mu\text{m}$ and $v_{\text{eff}} = 0.5$ (similar to the particle size distributions derived by Pollack *et al.* [1995] and Smith and Lemmon [1999]), which yields a visible to infrared optical depth ratio of approximately 1.5. Refractive indices are from Toon *et al.* [1977].

lengths. Figure 1 shows a plot of the dependence of the visible to infrared opacity ratio as a function of cross-section weighted mean particle size and effective width for spherical particles. Although the ratio increases with decreasing mean particle size and decreasing width of the distribution, the ratio never reaches values as high as those seen during the clear northern spring and summer seasons. Particle scattering calculations using nonspherical particles [Pollack and Cuzzi, 1980] can increase the ratio somewhat for a given effective radius (r_{eff}) and distribution width (v_{eff}); however, the increase does not reach the values seen in Plates 1b and 1e, except for distributions with very small effective radii and which are unrealistically narrow ($r_{\text{eff}} < 0.4 \mu\text{m}$ and $v_{\text{eff}} < 0.1$, Figure 1) (see Pollack *et al.* [1995] for a review).

It is interesting to consider the impact of a high visible to infrared ratio of optical depth on the behavior of an atmospheric model, assuming that dust provides the only source of opacity. We undertook such an experiment with the Geophysical Fluid Dynamics Laboratory Mars General Circulation Model [Wilson and Hamilton, 1996]. Specifically,

two numerical experiments were undertaken: first, a control simulation that was carefully tuned, through the rate of dust injection at the surface, so as to match Viking IRTM and Mariner 9 atmospheric temperature measurements; and second, an otherwise identical simulation with a visible to infrared opacity ratio of 12.5. In keeping with the fact that a high ratio corresponds to effective solar heating of the atmosphere and relatively ineffective cooling to space, a substantial (5–10 km deep) global inversion, absent in the control simulation (and hence the spacecraft data), was found to form near the surface of the high opacity ratio simulation in response to significant net heating due to dust. The effect of dust heating was noticeable throughout the atmosphere below roughly 50 km, with temperatures at 10 km being as much as 25 K warmer than those in the control simulation and 10 K warmer at 25 km. The deep inversion greatly reduced lower atmospheric convection and lead to a sharp reduction in dust lifting such that after 30 sols (Mars days) the opacities had dropped by a rough factor of 2 relative to the control simulation. In short, high dust visible to infrared

ratios do not appear to be consistent with the Martian atmosphere as we observe it [Zurek *et al.*, 1992], and thus a seasonal variation of the dust (as opposed to total aerosol) visible to infrared opacity ratio by the amounts suggested in Plates 1a and 1b is not physically credible.

A final argument against the dust particle size variation relates to the fact that if the visible to infrared optical depth ratio were varying significantly during the year due to dust alone, the spectral shape of the 9 μm silicate absorption feature should also change. In Figure 2, we show the variation of dust extinction in and around the 9 μm absorption feature for two combinations of ($r_{\text{eff}}, v_{\text{eff}}$): (0.3 μm , 0.0) and (1.8 μm , 0.5). These two combinations correspond to visible to infrared ratios of 6.5 and 1.5, respectively. There is a significant difference in the shape longward of 9.25 μm , and there is a noticeable secondary maxima in extinction at 8.8 μm in the former case, which is absent in the latter. However, analysis of recent Thermal Emission Spectrometer (TES) data [Smith *et al.*, 2000a; Bandfield *et al.*, 1999] has shown that the dust absorption spectra are fairly invariant with time (excluding the earliest phases of dust storms). This provides a strong indication that the dust particle size distribution is not varying significantly. Further, the absence of a secondary minima in most TES and Mariner 9 Infrared Interferometer Spectrometer (IRIS) spectra suggests that particle size variations cannot explain visible to infrared opacity ratios as large as 6.

3.2. Changes in the Vertical Distribution of Dust

Another potential explanation for the ratio variations relates to variations in depth to which dust is mixed. Specifically, it could be argued that if a uniform vertical distribution of dust is assumed in the retrieval of infrared opacities, while the true distribution had dust confined to relatively low heights in the atmosphere, the actual dust opacity would be underestimated by the retrieval, relative to dust distributed deeply through the atmosphere. Dust confined lower in the atmosphere is warmer and hence has a higher emission temperature. This results in a smaller difference in the brightness temperatures at 7 and 9 μm . Consequently, more dust (opacity) is needed to fit a given observed T_7 (7 μm brightness temperature) minus T_9 (9 μm brightness temperature) value in the confined dust case. In order to address this possibility we have modified the radiative scheme used by Martin [1986] and Martin and Richardson [1993] to treat arbitrary vertical dust distributions. The results for uniform, moderately confined (to 10 km), and shallowly confined (to 6 km) dust distributions are shown in Plates 1c and 1f. We did not consider dust distributions shallower than 6 km since at the low and mid-latitude landing sites, the daytime boundary layer depth should in general be roughly 6 km [Haberle *et al.*, 1993]. This effect of dust distribution assumption on the retrieval turns out to be rather small. It is <10% for clearer periods, increasing greatly during the dusty conditions of southern summer. However, during these periods the most likely case is a close to uniform distribution.

The explanation for the relatively small impact of the dust distribution assumption (for reasonable ranges) on retrieval

opacity is rather straightforward. "Uniform" dust refers to a constant dust mass mixing ratio as a function of height, which means that the total dust amount decreases exponentially with height (along with pressure). The difference between a uniform and a shallowly confined distribution is that while the dust amounts in the former decrease exponentially with height to the top of the atmosphere, the confined dust case has dust amounts decreasing exponentially to 6 km and decreasing more rapidly above that level. However, in both cases, the majority of the dust mass (and hence opacity) is located in the lowest half scale height of the atmosphere, where the distributions are very similar. In short, variation in dust vertical distribution cannot explain the magnitude of the observed variation in the visible to infrared opacity ratio.

3.3. Water Ice Hazes

These facts together suggest that the third hypothesis, added visible opacity due to water ice clouds, is more likely. Dusty periods lead to increases in atmospheric temperature, preventing the formation of water ice clouds. The clearer periods are colder, allowing water clouds to form more readily. Water ice clouds contribute opacity in visible wavelengths but much smaller amounts at the 7 and 9 μm wavelengths [Curran *et al.*, 1973; Smith *et al.*, 2000a] used for 9 μm optical depth retrieval, making the ratio of opacities increase. If we assume that the ratio of optical depth of dust (as opposed to total aerosol) in the visible to the infrared is truly 2.5, then Figure 3 shows the amount of opacity that is then due to water ice. Again it is important to note that we used daytime observations and therefore inferred water ice opacities and hence water ice mass estimates representative of daytime minimum values. The right-hand axis shows the amount of precipitable microns of water that is necessary to be frozen into ice in order to produce the required optical depth, using a modified gamma distribution ($r_{\text{eff}} = 0.3 \mu\text{m}$ and $v_{\text{eff}} = 0.03$, see section 4) and the water ice refractive indices of Warren [1984]. If the particle size distribution derived by Curran *et al.* [1973] ($r_{\text{eff}} = 2 \mu\text{m}$ and $v_{\text{eff}} = 0.03$) is used, the values shown on the right-hand axis of Figure 3 should be multiplied by 4. Similarly, if the ice grows around a dust core, concentric shell calculations [Bohren and Huffman, 1983] show that an ice mantle of roughly the same thickness as the original dust core radius is sufficient to make the composite dust/ice particle indistinguishable from pure ice in the visible and infrared. In this case the masses shown on the right-hand axis overestimate the true ice mass as the amount of water needed to grow around a dust core is less than the amount needed to grow a pure ice particle. The ice mass estimates are therefore likely only accurate to the order of magnitude level.

Although previous studies have assumed that water ice is negligible in the retrieval of 9 μm dust opacity, water ice can produce a spectral contrast between 7 and 9 μm . In Figure 4, we show the IRTM 7 and 9 μm channel brightness temperature differences possible for a range of water ice particle size distributions assuming a surface temperature of 250 K, an ice cloud temperature of 200 K, and an ice cloud opacity of 0.4 in the visible. In these calculations

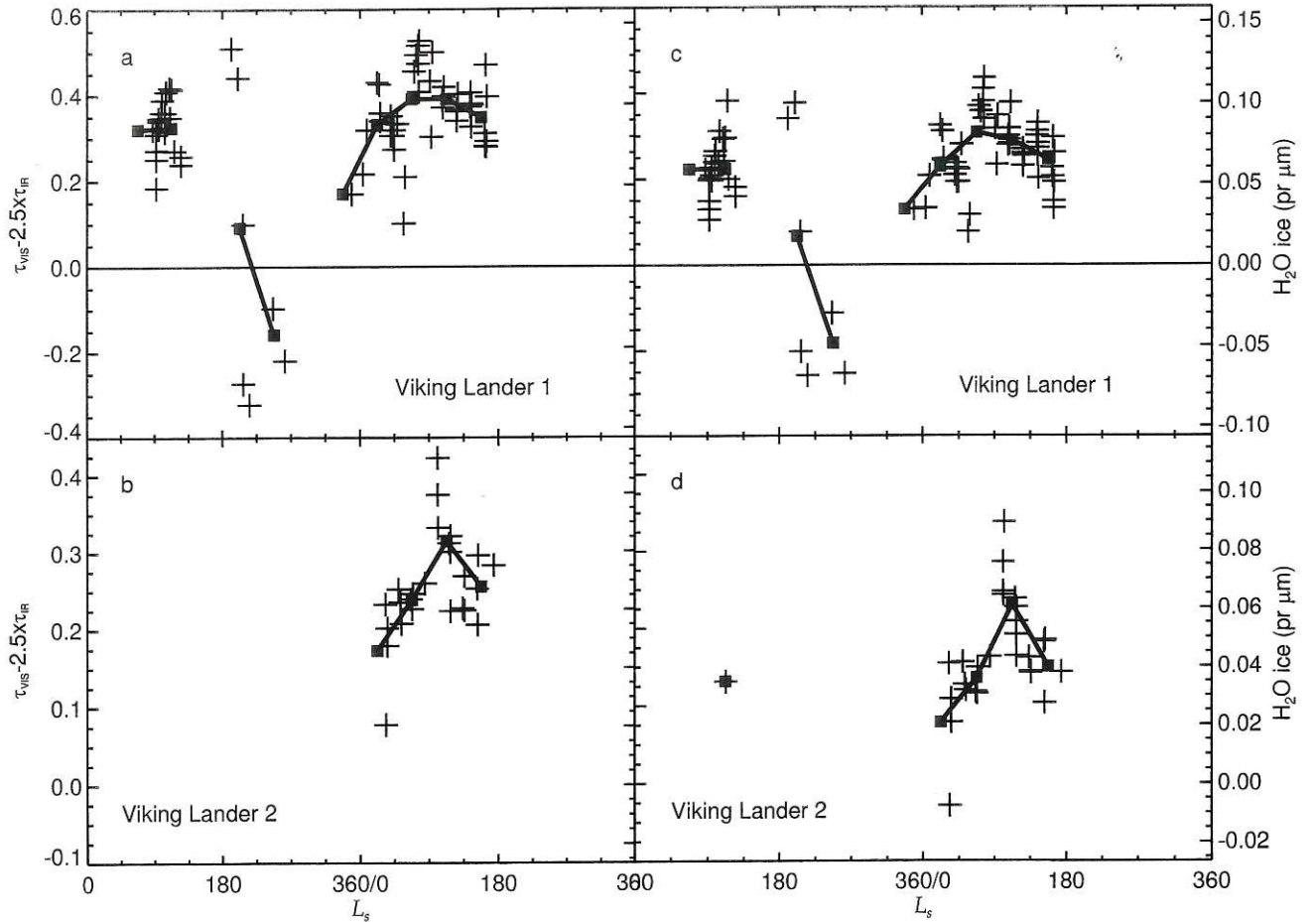


Figure 3. (a)–(b) Excess optical depth versus L_s for the Viking Lander 1 and 2 sites, respectively. Assuming the ratio of visible to infrared opacities for dust is a constant 2.5, $\tau_{\text{vis}} - 2.5 \tau_{\text{IR}}$ is a measure of the optical depth in the visible due to other opacity sources, such as water ice clouds. The boxes and lines are a boxcar average of all values in a $45^\circ L_s$ box. A size of 45° in L_s was used to span gaps in the temporal coverage; averages over a shorter interval follow the random noise, and averages over a longer interval damp out seasonal trends. It was also assumed that there is no relative difference in T_7 and T_9 brightness temperatures due to water ice and that vertical dust distribution is capped at 10 km. The right-hand axis corresponds to the right-hand axis in Figures 3c and 3d, and indicates the amount of precipitable microns of water that would need to be converted to water ice aerosols to produce the whole amount of excess optical depth, using a modified gamma distribution ($\alpha = 8$, $\gamma = 3$, $r_{\text{eff}} = 0.3 \mu\text{m}$, and $v_{\text{eff}} = 0.03$, see section 4) and the water ice optical parameters of Warren [1984]. (c)–(d) Excess optical depths similar to Figures 5a and 5b, except that a $T_7 - T_9$ difference of -1 K was assumed. The right hand axis shows the opacities converted to water ice amounts.

we have used the scattering and absorbing radiative model of *Paige et al.* [1994] and *Tamppari et al.* [2000]. These values represent the most extreme case (i.e., the case that will produce the largest ice cloud signal) that is still consistent with the opacity and IRTM temperature data. The $T_7 - T_9$ differences have a minimum value of approximately -1 K and are generally negative throughout most of the domain. The $T_7 - T_9$ values from the IRTM data set used in the determination of dust opacity typically have values between 0.7 and 1.5 K. Taking the extremum value of -1 K , from Figure 4, as the general impact of ice, suggests that the true $T_7 - T_9$ difference resulting solely from dust should be nearer 1.7 to 2.5 K. To test the impact of such $T_7 - T_9$ difference bias-

ing by ice, we retrieved the infrared dust optical depth for $T_7 - T_9$ values 1 K greater than is extracted from the IRTM data set. The resulting opacity values are shown in Figure 5 along with the standard values from Plates 1a and 1d. The increase in dust optical depth is only really significant during the relatively clear periods. Here the values increase from roughly 0.03–0.1 to 0.05–0.15. Applying the canonical dust opacity ratio of 2.5 and calculating the opacity deficit with respect to the visible opacity values, we derive new water ice opacities which are shown in Figures 3b and 3d. These values are now lower than those derived for the reference case since the dust provides a greater contribution to the total opacity in this case. Given the rather extreme surface-to-

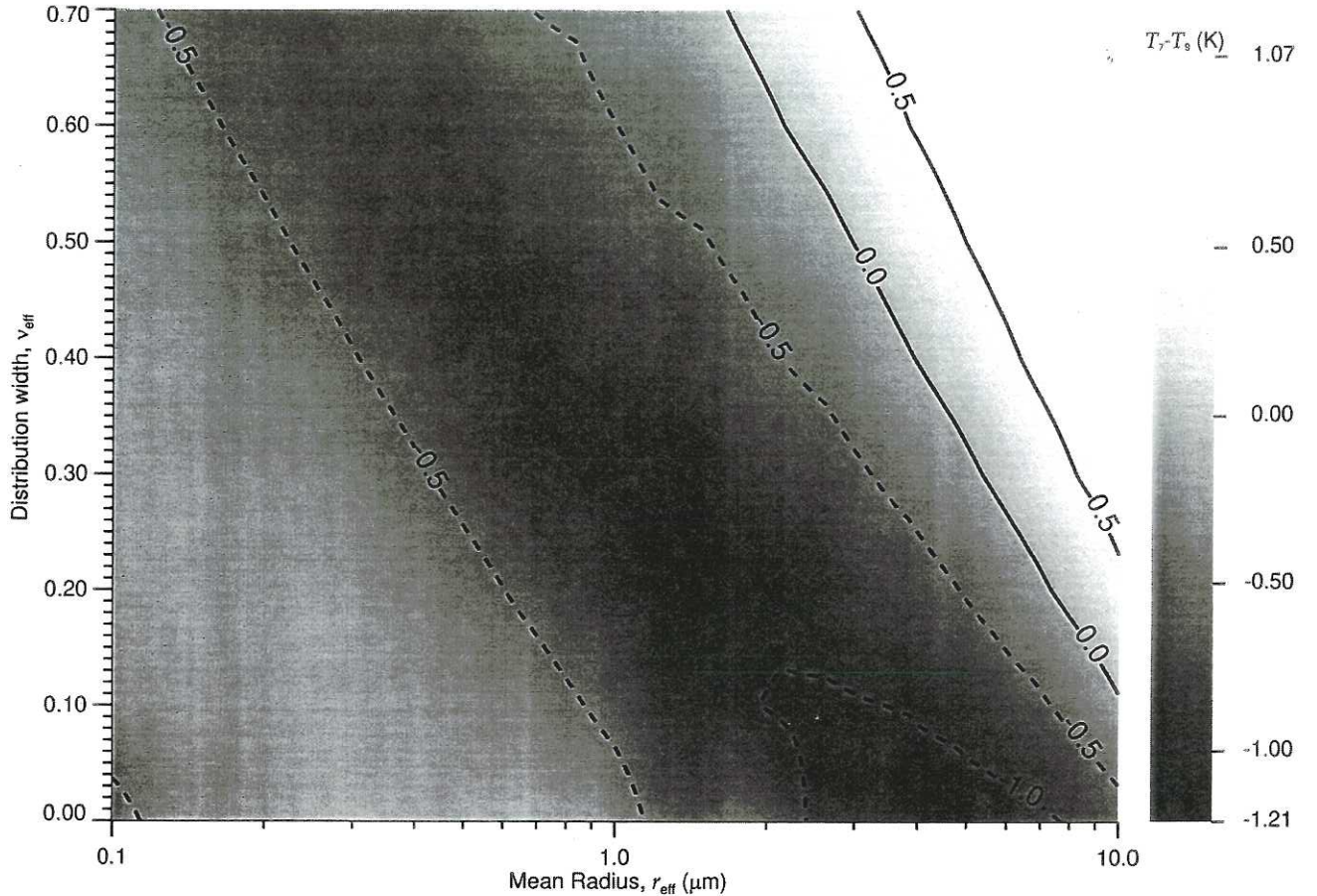


Figure 4. Difference between the IRTM T_7 (7 μm brightness temperature) and T_7 (9 μm brightness temperature) caused by water ice particles as a function of cross-section weighted mean particle size (r_{eff}), in microns, and effective width of the distribution (v_{eff}) for a modified gamma distribution of spherical dust particles. Indices of refraction came from Warren [1984]. The comment on the variables of the particle size distribution is the same as for Figure 1.

cloud temperature contrasts and the high ice opacity values used in deriving the higher dust amounts in this case, we can reasonably claim that the two cases shown in Figures 5 and 3 bound the true dust and water ice values during the Viking mission.

The wide spread of ice amounts at the VL sites during the dusty southern spring and summer seasons are caused by the difficulty of comparing the lander and orbiter observations of optical depth during a period of large and rapidly changing dust amounts. The IRTM observations are matched with a linearly interpolated lander opacity in order to calculate the visible to infrared opacity ratio, and thus the water ice amounts. This linear interpolation is valid during the relatively steady northern spring and summer, but introduces larger errors during the southern spring and summer periods of rapid change. However one can tell the visible and infrared values produce a good match, using the ratio of 2.5, based on simple visual inspection of Plate 1.

A seasonal cycle of cloudiness can now clearly be seen in the data, with cloud opacity disappearing during the dust storm periods and peaking during the northern spring and

summer. Although the data are noisy, the ice opacity values appear to peak around the northern solstice. There is even an indication that the peak at VL1 occurs earlier ($L_s=80^\circ-90^\circ$) than at VL2 ($L_s=115^\circ-130^\circ$). If true, these differences in timing may reflect a dependence of lower-latitude clouds on the strength of the overturning (Hadley) circulation, while the higher-latitude clouds respond more to the increasing vapor amounts. In any case this cycle of water ice is consistent with the cycle of water vapor observed by Mars Atmospheric Water Detector (MAWD) [Jakosky and Farmer, 1982], which peaks in the Northern Hemisphere during northern summer. A similar seasonal cycle of the apparition of water ice cloudiness and haziness has been reported by ground-based observers [Beish and Parker, 1990].

The values of “excess” optical depth due to water ice clouds in the Viking data as well as the values derived from the Mars Pathfinder data are of the order of a tenth to one precipitable micron. These are amounts that the atmosphere should have no difficulty supplying during these seasons given vapor amounts of a few tens of precipitable microns [Jakosky and Farmer, 1982]. The ice opacities we derive

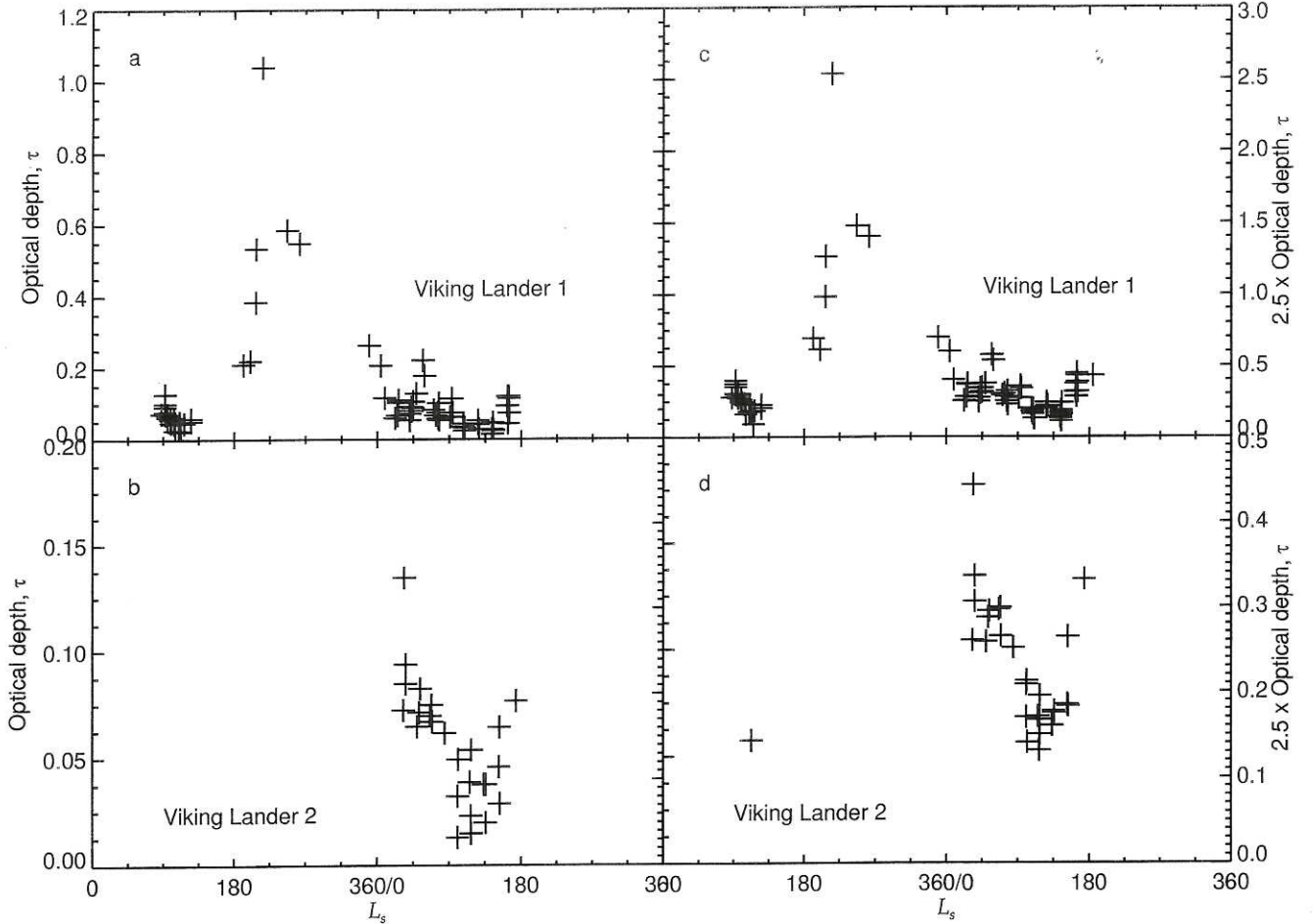


Figure 5. (a)–(b) Optical depths of dust in the infrared as a function of L_s for the Viking Lander 1 and 2 sites, respectively, assuming that there is no relative difference in T_7 and T_9 brightness temperatures due to water ice and that vertical dust distribution is capped at 10 km. The right-hand axis corresponds to the right-hand axis in Figures 5c and 5d, and shows the infrared values scaled by 2.5 for comparison with visible optical depths. (c)–(d) Dust optical depths in the infrared similar to Figures 5a and 5b, except that a $T_7 - T_9$ difference of -1 K was assumed to be due to water ice aerosols. The right hand axis shows the opacities scaled by 2.5 for comparison with the visible.

are consistent with measurements of water ice opacity made in the ultraviolet by Hubble Space Telescope [James *et al.*, 1996] after scaling for the difference in wavelength. It is also important to note that the ice amounts we derive refer to the daytime minimum values. Models suggest a diurnal cycle of cloud ice, involving up to a few precipitable microns [Richardson, 1999]. Our daytime derived values are not inconsistent with a cycle of this magnitude.

4. Reanalysis of Mars Pathfinder Optical Depths

Data from the Mars Pathfinder mission allow us to check our model of increased influence of water ice aerosols. The Imager for Mars Pathfinder (IMP) enabled the atmospheric optical depth to be measured at four wavelengths ($0.45, 0.67, 0.883$, and $0.989\text{ }\mu\text{m}$). Changes in the particle size distribution of dust and water ice will change their respective absorption spectra (derived from Mie scattering calculations)

at these wavelengths; consequently, the measured spectra can be used to constrain the particle size distributions of water ice and dust by shape fitting. Once the optimum distributions are computed, the mass fraction can be derived by matching to the total observed extinction. In this way we can test whether our picture of the seasonal variation of aerosols is consistent with the amount of dust and water ice opacity observed in the Mars Pathfinder measurements.

The IMP observations [Smith and Lemmon, 1999] show a similar amount of dust in the $0.67\text{ }\mu\text{m}$ region as the VL measurements for the 90 sols for which they operated ($L_s = 143^\circ - 188^\circ$). In general, IMP saw similar or slightly higher optical depth in the blue filter compared to the red filter. Smith and Lemmon [1999] account for this extra opacity in the blue wavelengths with high-altitude Rayleigh-scattering ice particles. They note that this solution is not unique, and indeed, we found that a haze of low-altitude ice particles also provides a fit to their wavelength-dependent observations.

We used the dust particle size distribution derived by

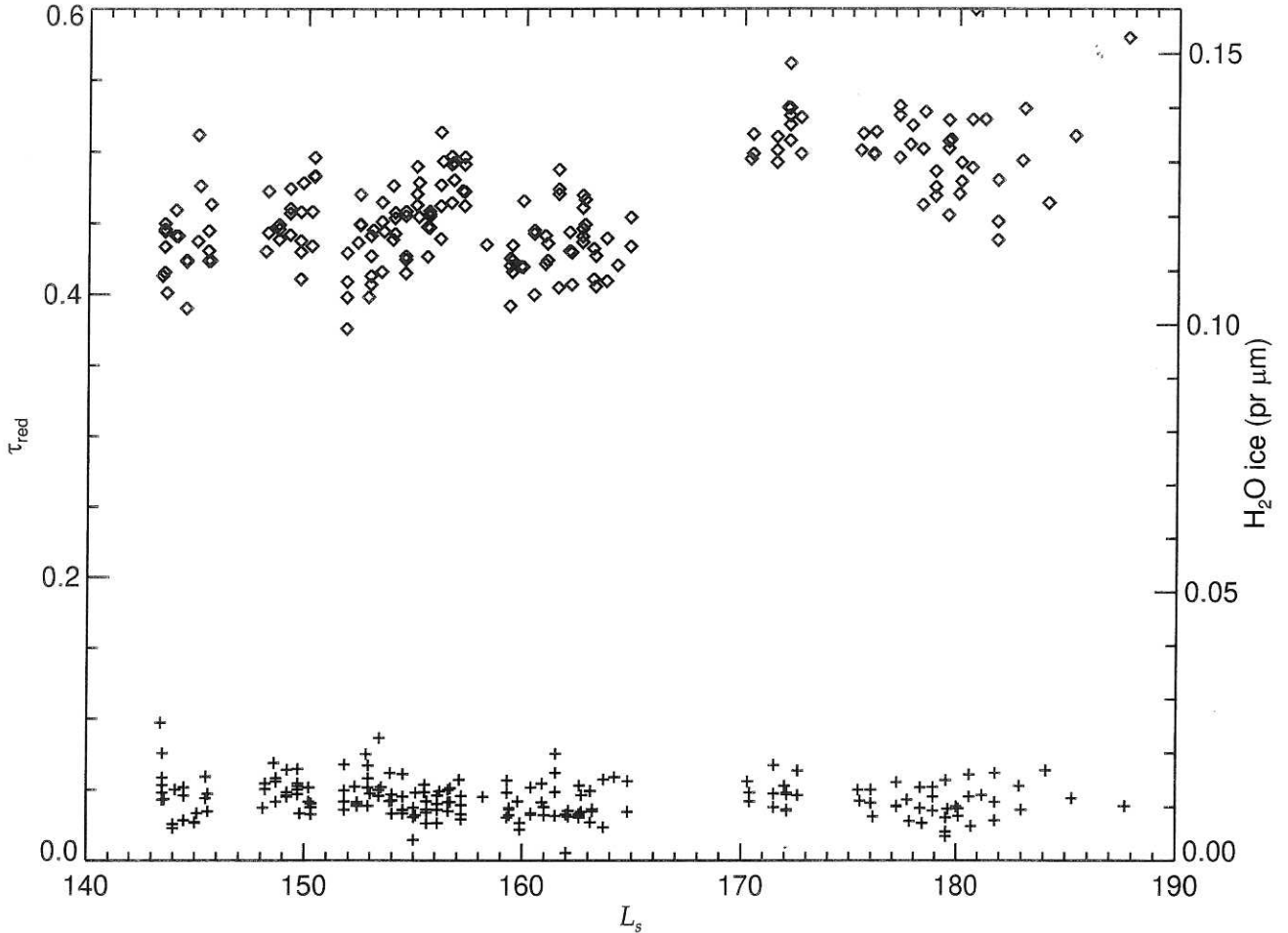


Figure 6. Derived values of optical depths of dust and ice in the red ($0.67 \mu\text{m}$) versus L_s for Mars Pathfinder. Only measurements made during the afternoon (after 1200 LT and before 1800 LT) were used in order to remove the diurnal water ice cycle. Diamonds are the dust optical depth, and crosses are the water ice optical depth (where optical depth solutions of 0.0 for ice have not been plotted). The particle size distribution of Tomasko *et al.* [1999] ($r_{\text{eff}} = 1.6 \mu\text{m}$ and $v_{\text{eff}} = 0.6$) was used for dust, while a modified gamma distribution with $r_{\text{eff}} = 0.3 \mu\text{m}$ and $v_{\text{eff}} = 0.03$ ($\alpha = 8$ and $\gamma = 3$) was used for ice. Refractive indices of Ockert-Bell *et al.* [1997] and Warren [1984] were used for dust and ice, respectively. These solutions were constrained by total optical depth measurements in the 0.45 , 0.67 , 0.883 , and $0.989 \mu\text{m}$ filters. The right-hand axis indicates the amount of precipitable microns of water that would need to be converted to water ice aerosols to produce the water ice optical depth seen using the above mentioned ice distribution.

Tomasko *et al.* [1999] based upon the angular dependence of the Pathfinder spectral observations. The effective mean radius of their distribution ($r_{\text{eff}} = 1.6 \mu\text{m}$) is in good agreement with previous Viking and Phobos measurements (see Pollack *et al.* [1995] for a summary), but they were unable to constrain the distribution width beyond a value of $v_{\text{eff}} \geq 0.2$. We thus experimented with a range of dust distribution widths and with both the effective radius and width of water ice distributions. We found that the ice distribution specified by Curran *et al.* [1973] is unable to fit the Pathfinder opacity observations regardless of the dust distribution width. In fact, only ice distributions with an effective particle size $\leq 0.5 \mu\text{m}$ were capable of producing a fit, in combination with the dust distribution of Tomasko *et al.*

[1999]. The width of the ice distribution was found to have a negligible effect on the quality of the fit or the derived dust/ice fraction. In addition, we found that the best fit to the Pathfinder data, regardless of the ice distribution, was obtained with a dust distribution v_{eff} of 0.6. This is within the range specified by Tomasko *et al.* [1999] and should be viewed as a refinement of their estimate.

The Viking data for the Pathfinder observation period now allow us to constrain the ice particle size effective radius even further. The VL1 data for the Pathfinder period suggest a water ice contribution of optical depth in the $0.67 \mu\text{m}$ channel of $0.0 - 0.1$. We found that an effective radius of $0.3 \pm 0.1 \mu\text{m}$ produces red optical depths within this range. Figure 6 shows our solution for the amount of ice and dust

necessary to fit both the Pathfinder and VL1 measurements of optical depth.

5. Current State of the Martian Climate

One of the primary results of the Viking mission was a detailed description of the current Martian climate. The annual cycles of atmospheric temperature, dust, and volatiles were defined by observations spanning several Martian years. However, *Clancy et al.* [1990, 1996] have recently suggested that this picture may not be representative of every, or even most, years. Specifically, they claimed that the bulk Martian atmosphere near 25 km is now (1980–present) cooler by roughly 15–20 K than during the Viking period (1976–1980). Based upon Hubble Space Telescope observations, they also suggested that Mars is less dusty than was observed during the Viking era and emphasized both the presence of water ice clouds and their potential role in limiting the vertical distribution of dust (hence reducing atmospheric temperatures through decreased solar absorption).

It is now known that the Martian climate has not changed significantly between the Viking mission and more recent times [Richardson, 1998]. The discrepancy between air temperatures derived from Viking IRTM measurements and those derived from ground-based observations results from a systematic warm bias in the Viking observations [Wilson and Richardson, 2000]. The Viking year mean air temperatures now appear to agree with the more recent TES [Conrath et al., 1999] and microwave observations [Clancy et al., 2000]. However, both the Mars Pathfinder [Smith and Lemmon, 1999] and TES [Smith et al., 2000b] measurements of optical depth were found to be in good agreement with Viking values. At first glance this would appear to be inconsistent with the downward revision of atmospheric temperatures, especially during the cool northern spring and summer seasons. Agreement between Viking and Pathfinder visible optical depths results mainly from the fact that the Pathfinder observations occurred during the late northern summer, when atmospheric water ice constitutes a small fraction of the atmospheric aerosol load. For northern spring and summer the inconsistency is resolved by the recognition that previous analysis of the Viking visible optical depth measurements overestimated dust optical depths and by neglecting the water ice opacity. Thus the “new” picture of the Viking era includes lower atmospheric temperatures, lower dust opacities, and more atmospheric water ice.

The results of this study suggest that at least the northern spring and summer seasons are less dusty than generally interpreted, based on the Viking Lander observations. In addition, we suggest that there is significant seasonal variation in the ubiquitous water ice haze. This latter suggestion is in keeping with recent Mars Orbiter Camera (MOC) [Malin et al., 1998] and TES (J.C. Pearl et al., Mars Global Surveyor Thermal Emission Spectrometer observations of water ice clouds during aerobraking and science phasing, submitted to *Journal of Geophysical Research*, 1999) observations and reanalysis of Viking IRTM data [Tamppari et al., 2000], which show rather widespread haziness due to water ice.

In general, evidence suggests a rather repeatable northern spring and early summer [Richardson, 1998; Clancy et al., 2000; Martin and Richardson, 1993; Smith et al. 2000b] and a downward revision of visible dust opacities during these seasons would appear to help in reconciling atmospheric temperature and dust observations.

6. Summary and Conclusions

We have rederived 9 μm optical depths from the Viking IRTM data and compared them with measurements of visible opacity from the Viking Landers. We found that the ratio of visible to infrared opacity, which is typically assumed to be constant, varies significantly with season. Both the visible and infrared opacities are usually assumed to relate only to the dust amount in the atmosphere. Indeed, we investigated two potential explanations for the opacity ratio variations that involve only variations in the dust properties. The first argues that variations in dust particle sizes affect the ratio. However, we show that realistic particle size variations can explain less than half the range in the derived opacity ratios, that even these variations do not appear to be reasonable based on TES observations, and that such high ratios of visible-to-infrared dust opacity would result in an unrealistic atmospheric temperature structure and circulation. The second potential explanation argues that if dust is confined low in the atmosphere, our retrieval scheme (which assumes uniformly mixed dust) would underestimate the true infrared dust opacity. In this case the true opacity ratio would remain constant, but would appear to vary due to errors in our infrared opacity calculation. We modified our retrieval scheme to treat nonuniform dust, but found this explanation able to account for only 10% of the peak opacity ratio variation, even for dust confined to an unrealistically shallow column.

We conclude that the most likely explanation for variations in the opacity ratio is the previously neglected role of persistent water ice hazes and clouds during northern spring and summer. The implication here is that the Viking-derived visible and infrared optical depths are not representative of the seasonal cycle of dust, but of the combined cycles of dust and atmospheric water ice. Thus we conclude that Mars is less dusty and more cloudy than was believed on the basis of VL observations, especially during the northern spring and summer seasons. Visible optical depths during the northern spring and summer seasons are typically 0.1–0.4 for dust and 0.1–0.4 for water ice, during the daytime. During the rest of the year the water ice visible opacities fall below 0.1, while dust opacities vary greatly, but generally are above 0.4. The variations in dust and water ice opacities appear to be strongly anticorrelated. The ice amounts peak in early northern summer (with the opacities possibly peaking earlier at VL1 than at VL2), while the dust opacity is a minimum at these times. The ice mass amounts derived from the peak ice opacities are sensitive to ice particle sizes, but are of order 0.1–0.5 pr. μm . This is roughly 1–5% of the total water column.

Using both the Pathfinder and Viking data, we also have been able to place a tighter constraint on the dust particle

size distribution of Tomasko *et al.* [2000] ($r_{\text{eff}} = 1.6 \mu\text{m}$ and $v_{\text{eff}} = 0.6$), and to derive the background water ice size distribution ($r_{\text{eff}} = 0.3 \mu\text{m}$ and $v_{\text{eff}} = 0.03$). However, the ice particle size distribution may change as a function of season. In addition, we suggest that for dust the ratio of optical depth in the infrared to the visible is likely to lie near 2.5 and that consequently, models which use this constant value are likely not in error.

Acknowledgments. We would like to thank Terry Z. Martin, John Pearl, and Eric Winter for the provision of the original dust retrieval algorithm and for useful discussion of both the data and the code. We would also like to thank Leslie Tamppari and an anonymous reviewer for useful comments and suggestions that greatly improved the paper. We would like to thank Todd Clancy for suggesting that we investigate the role of vertical dust distribution on retrieved infrared opacity values. Finally, we would like to thank Andy Ingersoll, Ashwin Vasavada, and R. John Wilson for useful and constructive discussions.

References

- Bandfield, J. L., P. R. Christensen, and M. D. Smith, Spectral data set factor analysis and end-member recovery: Application to analysis of Martian atmospheric particulates, *J. Geophys. Res.*, in press, 1999.
- Beish, J. D., and D. C. Parker, Meteorological survey of Mars, 1969–1984, *J. Geophys. Res.*, 95, 14,657–14,675, 1990.
- Bohren, C. F., and D. R. Huffman, *Absorption and Scattering of Light by Small Particles*, Wiley, New York, 1983.
- Christensen, P. R., Martian dust mantling and surface composition: Interpretation of thermophysical properties, *J. Geophys. Res.*, 87, 9985–9998, 1982.
- Clancy, R. T., D. O. Muhleman, and G. L. Berge, Global changes in the 0–70 km thermal structure of the Mars atmosphere derived from 1975 to 1989 microwave CO spectra, *J. Geophys. Res.*, 95, 14,543–14,554, 1990.
- Clancy, R. T., A. W. Grossman, M. J. Wolff, P. B. James, D. J. Rudy, Y. N. Billawala, B. J. Sandor, S. W. Lee, and D. O. Muhleman, Water vapor saturation at low altitudes around Mars aphelion: A key to Mars climate?, *Icarus*, 122, 36–62, 1996.
- Clancy, R. T., B. J. Sandor, M. J. Wolff, P. R. Christensen, M. D. Smith, J. C. Pearl, B. J. Conrath, and R. J. Wilson, An intercomparison of ground-based millimeter, MGS TES, and Viking atmospheric temperature measurements: Seasonal and interannual variability of temperatures and dust loading in the global Mars atmosphere, *J. Geophys. Res.*, in press, 2000.
- Colburn, D. S., J. B. Pollack, and R. M. Haberle, Diurnal variations in optical depth at Mars, *Icarus*, 79, 159–189, 1989.
- Conrath, B. J., Thermal structure of the Martian atmosphere during the dissipation of the dust storm of 1971, *Icarus*, 24, 36–46, 1975.
- Conrath, B. J., J. C. Pearl, M. D. Smith, W. C. Maguire, S. Da son, M. S. Kaelberer, and P. R. Christensen, Mars Global Surveyor Thermal Emission Spectrometer (TES) observations: Atmospheric temperatures during aerobraking and science phasing, *J. Geophys. Res.*, in press, 1999.
- Curran, R. J., B. J. Conrath, R. A. Hanel, V. G. Kunde, and J. C. Pearl, Mars: Mariner 9 spectroscopic evidence for H_2O ice clouds, *Science*, 182, 381–383, 1973.
- Fenton, L. K., J. C. Pearl, and T. Z. Martin, Mapping Mariner 9 dust opacities, *Icarus*, 130, 115–124, 1997.
- Haberle, R. M., H. C. Houben, R. Hertenstein, and T. Herdtle, A boundary layer model for Mars: Comparison with Viking Lander and entry data, *J. Atmos. Sci.*, 50, 1544–1559, 1993.
- Herr, K. C., and G. C. Pimental, Evidence for solid carbon dioxide in the upper atmosphere of Mars, *Science*, 167, 496–499, 1969.
- Jakosky, B. M., and C. B. Farmer, The seasonal and global behavior of water vapor in the Mars atmosphere: Complete global results of the Viking atmospheric water detector experiment, *J. Geophys. Res.*, 87, 2999–3019, 1982.
- James, P. B., J. F. Bell III, R. T. Clancy, S. W. Lee, L. J. Martin, and M. J. Wolff, Global imaging of Mars by Hubble space telescope during the 1995 opposition, *J. Geophys. Res.*, 101, 18,883–18,890, 1996.
- Kahn, R., R. Goody, and J. Pollack, The Martian twilight, *J. Geophys. Res.*, 86, 5833–5838, 1981.
- Malin, M. C., et al., Early views of the Martian surface from the Mars orbiter camera of Mars Global Surveyor, *Science*, 279, 1681–1685, 1998.
- Martin, T. Z., Thermal infrared opacity of the Mars atmosphere, *Icarus*, 66, 2–21, 1986.
- Martin, T. Z., and M. I. Richardson, New dust opacity mapping from Viking infrared thermal mapper data, *J. Geophys. Res.*, 98, 10,941–10,949, 1993.
- Ockert-Bell, M. E., J. F. Bell III, J. B. Pollack, C. P. McKay, and F. Forget, Absorption and scattering properties of the Martian dust in the solar wavelengths, *J. Geophys. Res.*, 102, 9039–9050, 1997.
- Paige, D. A., J. E. Bachman, and K. D. Keegan, Thermal and albedo mapping of the polar regions of Mars using Viking thermal mapper observations. 1. North polar region, *J. Geophys. Res.*, 99, 25,959–25,991, 1994.
- Pollack, J. B., and J. N. Cuzzi, Scattering by nonspherical particles of size comparable to a wavelength: A new semi-empirical theory and its application to tropospheric aerosols, *J. Atmos. Sci.*, 37, 868–881, 1980.
- Pollack, J. B., D. S. Colburn, R. Kahn, J. Hunter, W. V. Camp, C. E. Carlson, and M. R. Wolf, Properties of aerosols in the Martian atmosphere, as inferred from Viking Lander imaging data, *J. Geophys. Res.*, 82, 4479–4496, 1977.
- Pollack, J. B., D. S. Colburn, M. Flasar, R. Kahn, C. E. Carlson, and D. Pidek, Properties and effects of dust particles suspended in the Martian atmosphere, *J. Geophys. Res.*, 84, 2929–2945, 1979.
- Pollack, J. B., M. E. Ockert-Bell, and M. K. Shepard, Viking Lander image analysis of Martian atmospheric dust, *J. Geophys. Res.*, 100, 5235–5250, 1995.
- Richardson, M. I., Comparison of microwave and infrared measurements of Martian atmospheric temperatures: Implications for short-term climate variability, *J. Geophys. Res.*, 103, 5911–5918, 1998.
- Richardson, M. I., A general circulation model study of the Mars water cycle, Ph.D. thesis, University of California, Los Angeles, 1999.
- Smith, M. D., J. L. Bandfield, and P. R. Christensen, Separation of atmospheric and surface spectral features in Mars Global Surveyor Thermal Emission Spectrometer (TES) spectra, *J. Geophys. Res.*, in press 2000a.
- Smith, M. D., J. C. Pearl, B. J. Conrath, and P. R. Christensen, Mars Global Surveyor Thermal Emission Spectrometer (TES) observations of dust opacity during aerobraking and science phasing, *J. Geophys. Res.*, in press 2000b.
- Smith, P. H., and M. Lemmon, Opacity of the Martian atmosphere measured by the Imager for Mars Pathfinder, *J. Geophys. Res.*, 104, 8975–8985, 1999.
- Tamppari, L. K., R. W. Zurek, and D. A. Paige, Viking era water ice clouds, *J. Geophys. Res.*, in press 2000.
- Tomasko, M. G., L. R. Doose, M. Lemmon, P. H. Smith, and E. Wegryn, Properties of dust in the Martian atmosphere from the Imager on Mars Pathfinder, *J. Geophys. Res.*, 104, 8987–9007, 1999.
- Toon, O. B., J. B. Pollack, and C. Sagan, Physical properties of the particles composing the Martian dust storm of 1971–1972, *Icarus*, 30, 663–696, 1977.

- Warren, S. G., Optical constants of ice from the ultraviolet to the microwave, *Appl. Opt.*, 23, 1206–1225, 1984.
- Wilson, R. J., and K. Hamilton, Comprehensive model simulation of thermal tides in the Martian atmosphere, *J. Atmos. Sci.*, 53, 1290–1326, 1996.
- Wilson, R. J., and M. I. Richardson, The Martian atmosphere during the Viking Mission, 1: Infrared measurements of atmospheric temperatures revisited, *Icarus*, in press, 2000.
- Zurek, R. W., Inference of dust opacities for the 1977 Martian great dust storms from Viking Lander 1 pressure data, *Icarus*, 45, 202–215, 1981.
- Zurek, R. W., J. R. Barnes, R. M. Haberle, J. B. Pollack, J. E. Tillman, and C. B. Leovy, Dynamics of the atmosphere of Mars, in *Mars*, edited by H. H. Kieffer, B. M. Jakosky, C. W. Snyder, and M. S. Matthews, pp. 835–933, Univ. of Ariz. Press, Tucson, 1992.
-
- M. I. Richardson and A. D. Toigo, Division of Geological and Planetary Sciences, MS 150-21, California Institute of Technology, Pasadena, CA 91125. (mir@gps.caltech.edu; toigo@gps.caltech.edu)

(Received June 28, 1999; revised November 3, 1999; accepted November 9, 1999.)

